Available online at www.sciencedirect.com
ScienceDirect
Journal of Catalysis 252 (2007) 312–320
JOURNAL OF CATALYSIS
www.elsevier.com/locate/jcat

Effect of pore size on the performance of mesoporous material supported chiral Mn(III) salen complex for the epoxidation of unfunctionalized olefins

Kai Yu [a,b], Zhicheng Gu [a,b], Runan Ji [a,b], Lan-Lan Lou [a,b], Fei Ding [a,b], Cui Zhang [a,b], Shuangxi Liu [a,b,*]

[a] *Institute of New Catalytic Materials Science, College of Chemistry, Nankai University, Tianjin 300071, PR China*
[b] *State Key Laboratory of Elemento-organic Chemistry, Nankai University, Tianjin 300071, PR China*

Received 26 July 2007; revised 13 September 2007; accepted 13 September 2007

Available online 23 October 2007

Abstract

A series of mesoporous MCM-41 and MCM-48 materials with different pore sizes were synthesized and used as supports to immobilize chiral Mn(III) salen complex. The heterogeneous catalysts were characterized by XRD, FT-IR, DR UV–vis, and N_2 sorption, and the results indicated the successful immobilization of chiral Mn(III) salen complex. The confinement effect of pore size on the catalytic performance of the heterogeneous catalysts was studied for the asymmetric epoxidation of unfunctionalized olefins with *m*-chloroperoxybenzoic acid as an oxidant. It was found that the conversions and enantiomeric excess (ee) values were closely correlated with the pore sizes of parent supports. The catalysts immobilized on the large-pore mesoporous supports exhibited higher conversions, and for the catalysts immobilized on MCM-41 materials, the ee values improved with increasing pore size. However, for the MCM-48 material-supported catalysts, the compatible pore size of the support with the substrate was beneficial for obtaining higher enantioselectivity in olefin epoxidation.

Keywords: Confinement effect; Pore size; Mesoporous materials; Chiral Mn(III) salen complex; Immobilization; Asymmetric epoxidation; Unfunctionalized olefins

1. Introduction

The asymmetric epoxidation of unfunctionalized olefins is an important reaction for synthesizing a variety of valuable chiral building blocks that can be easily transformed into other useful chiral compounds through regioselective ring-opening reactions [1], and thus is widely used in the synthesis of pharmaceuticals and agrochemicals. Chiral Mn(III) salen complexes have demonstrated activity and selectivity for the enantioselective epoxidation of unfunctionalized olefins under both homogeneous [2,3] and heterogeneous [4–11] conditions. However, in general, the expensive catalysts are quite difficult to separate and recycle in homogeneous catalytic systems. In recent years, the heterogenization of chiral Mn(III) salen complexes within inorganic matrixes has received much attention [12–24] due to the advantages of heterogeneous catalysis systems, including easy catalyst/product separation and simple catalyst recycling.

Many kinds of mesoporous materials with large surface areas and controllable pore sizes of 2–50 nm were used as matrixes to immobilize chiral Mn(III) salen complexes, which allows easy diffusion of reactants to the active sites located on the inner surface. Moreover, these mesoporous materials can be easily organically functionalized due to the abundant silanol groups on their surface. Over the last decade, several different strategies have been adopted to immobilize chiral Mn(III) salen complexes on mesoporous materials. Zhang et al. [13,14] reported a new method of axially immobilizing chiral Mn(III) salen complexes through a phenyl sulfonic group onto the surface of mesoporous supports, which led to an improved enantiomeric excess (ee) over that of the free complex. Kureshy et al. successfully immobilized chiral Mn(III) salen complexes on pyridine *N*-oxide-modified mesoporous supports through axial coordination [15] and on aminopropyl-modified mesoporous supports through covalent grafting [16]. An effective approach based on supported ionic liquid was reported by Lou

* Corresponding author. Fax: +86 22 23509005.
E-mail address: sxliu@nankai.edu.cn (S. Liu).

0021-9517/$ – see front matter
doi:10.1016/j.jcat.2007.09.009

et al. [17,18] for the immobilization of chiral Mn(III) salen complexes on mesoporous materials, and excellent catalytic performance was obtained for the immobilized catalysts. The chiral Mn(III) salen complexes were immobilized on MCM-41 [19] and MCM-48 [20,21] through a multistep grafting method. The ion-exchange method was reported to immobilize chiral Mn(III) salen complexes on Al-MCM-41 [22–24].

In most cases, the heterogenized chiral Mn(III) salen catalysts led to lower activity and enantioselectivity compared with the homogeneous counterparts for asymmetric epoxidation, and only a few heterogeneous catalysts have exhibited higher ee values than the homogeneous ones. The improvement of enantioselectivity was mainly attributed to the confinement effect of supports in these literatures [12–17,20], which was also proposed for other heterogeneous asymmetric reactions by Thomas et al. [25] and Caplan et al. [26]. However, the effect of pore size on the catalytic performance of mesoporous material-supported chiral Mn(III) salen complex has seldom been systemically investigated for the heterogeneous asymmetric epoxidation. In this work, a series of mesoporous MCM-41 and MCM-48 materials with different pore sizes were synthesized and used as supports to immobilize chiral Mn(III) salen complex. The as-synthesized catalysts were used in the epoxidation of unfunctionalized olefins with the combination of *m*-chloroperbenzoic acid (*m*-CPBA) and *N*-methylmorpholine-*N*-oxide (NMO) as the oxidant system, which could achieve excellent catalytic performance rapidly. The effect of the nanopores of the supports on activity and enantioselectivity of the heterogeneous catalysts was studied.

2. Experimental

2.1. General

Tetraethyl orthosilicate (TEOS; AR), alkyltrimethylammonium bromide $C_nH_{2n+1}(CH_3)_3$–NBr (C_nTAB for brevity, $n = 12, 14, 16, 18$; AR), ammonia (25 wt%; AR), and sodium hydroxide (NaOH; AR) were used to prepare siliceous mesoporous materials. 1-Phenylcyclohexene, NMO and α-methylstyrene were provided by Aldrich. Indene was obtained from Fluka. 3-Aminopropyltriethoxysilane and *m*-CPBA were purchased from Acros Organics. *Cis*/*trans*-1,2-diaminocyclohexane and 2-*tert*-butylphenol were supplied by Alfa Aesar. 3-*tert*-Butyl-2-hydroxybenzaldehyde was synthesized from 2-*tert*-butylphenol as described previously [27]. (1*R*, 2*R*)-(-)-1,2-Diaminocyclohexane was resolved from the technical grade isomers mixture in >99% enantiomeric excess by the reported procedure [28]. All of the solvents used in the present study were purified before use.

Racemic epoxides were synthesized by the epoxidation of corresponding olefins with *m*-CPBA in $CHCl_3$ at 273 K [29] and detected by gas chromatography (GC). The conversions (with toluene as internal standard) and ee values of epoxidation reaction were determined by GC with a chiral β-cyclodextrin capillary column (RESTEK RT-BetaDEXse, 30 m × 0.25 mm × 0.25 μm), using a Rock GC7800 gas chromatograph equipped with a flame ionization detector. Ultrapure nitrogen was used as the carrier gas with the injection port temperature set at 523 K. The column temperature for styrene, α-methylstyrene, and indene was programmed in the range of 333–423 K, and for 1-phenylcyclohexene, the temperature was in the range of 353–423 K. For each of the epoxidation reactions, the conversion and ee value were determined by averaging the values from two parallel measurements, of which the results should not differ by more than 0.5%, otherwise additional measurements on the same sample need to be done. ^{1}H and ^{13}C {^{1}H} NMR spectra were recorded at 300 and 75 MHz, respectively, using a Varian Mercury Vx-300 spectrometer. Elemental analysis was conducted with a Perkin–Elmer 240C analyzer. Mass spectra were performed on a VG ZAB-HS (FAB) spectrometer. The content of Mn in the heterogeneous catalysts was determined by inductively coupled plasma–atomic emission spectrometry (ICP-AES) on an ICP-9000 (N + M) spectrometer (TJA Co.), after the samples were calcined and dissolved in hydrogen fluoride. Powder X-ray diffraction (XRD) patterns of the samples were obtained on a R/max-2500 diffractometer with Cu$K\alpha$ radiation (40 kV and 100 mA) in a scan range of $0.6° < 2\theta < 80°$. FT-IR spectra were recorded on KBr pellets in a BRUKER VECTOR 22 spectrometer in the region of 400–4000 cm^{-1}. Diffuse-reflectance UV–vis (DR UV–vis) spectra were obtained on a Shimadzu UV-2550 UV–vis spectrophotometer in the range of 220–800 nm. N_2 adsorption–desorption analysis was carried out at 77 K on a Micromeritics TriStar 3000 apparatus. The analytical data were processed by the BET equation for surface areas and by the BJH model for pore size distributions.

2.2. Synthesis of siliceous mesoporous materials

2.2.1. Synthesis of MCM-41 with different pore sizes

A series of highly ordered hexagonal siliceous MCM-41 with different pore sizes were synthesized according to the literature method [30,31]. The alkylammonium salts C_nTAB ($n = 12, 14, 16, 18$) with different alkyl chain lengths and TEOS were used as template and silica source, respectively. A gel (molar) composition of $1TEOS/0.12C_nTAB/8NH_4OH/114H_2O$ was used. In a typical synthesis, the template of C_nTAB was dissolved in warm deionized water, and the ammonia was added to this solution under vigorous stirring. The required quantity of TEOS was then added dropwise into the solution. After 0.5 h of stirring at room temperature, the resulting gel was allowed to crystallize at 383 K for 52 h in a Teflon-lined autoclave. The solid product was recovered by filtration, washed with deionized water, dried at room temperature, and calcined at 823 K in air for 6 h to remove the template. According to the differences in the alkyl chain length of the template, the as-synthesized materials were marked as *n*MCM-41 ($n = 12, 14, 16, 18$).

2.2.2. Synthesis of MCM-48 with different pore sizes

The alkylammonium salts C_nTAB ($n = 12, 14, 16$) with different alkyl chain lengths were used as templates to synthesize the siliceous MCM-48 with different pore sizes. When C_nTAB ($n = 14, 16$) was used as template, a typical synthesis procedure was carried out as follows [30,31]. The template

of C_nTAB was dissolved in warm deionized water, and to this solution the required quantity of TEOS and the aqueous solution of NaOH were added orderly under vigorous stirring. After stirring for another 2 h, a gel with a molar composition of 1TEOS/0.46C_nTAB/0.41NaOH/52.95H_2O was obtained. The resulting gel was allowed to crystallize at 383 K for 72 h in a Teflon-lined autoclave. The solid product was recovered by filtration, washed with deionized water, and dried in air at room temperature overnight. The template was removed by calcination at 823 K in air for 6 h. According to the difference of the chain length of the template, the as-synthesized materials were marked as *n*MCM-48 ($n = 14$, 16).

When C_nTAB ($n = 12$) was used as template, the synthesis procedure was carried out as follows. The template of C_{12}TAB was dissolved in warm deionized water, and the NaOH aqueous solution was added to this solution under stirring. Then the required quantity of TEOS was added dropwise into the solution. After stirring for 0.5 h at room temperature, a gel with a molar composition of 1TEOS/1.10C_nTAB/0.46NaOH/112H_2O was obtained. The gel was then transferred into a Teflon-lined autoclave for crystallization at 393 K for 168 h. The solid product was recovered by filtration, washed with deionized water, dried at room temperature, and calcined at 823 K in air for 6 h to remove the template. The as-synthesized material was marked as *n*MCM-48 ($n = 12$).

2.3. Synthesis of the homogeneous chiral Mn(III) salen complex *1*

The chiral Mn(III) salen complex **1** was obtained through the synthesis sequence given in Scheme 1. A mixture of 3-*tert*-butyl-2-hydroxybenzaldehyde (**A**) (2.7 g, 15.2 mmol), paraformaldehyde (1.0 g, 33.3 mmol), and tetrabutylammonium bromide (0.47 g, 1.46 mmol) in 11 ml of concentrated hydrochloric acid was stirred vigorously at 313 K for 3 days [32]. The reaction mixture was repeatedly extracted with diethyl ether (3 × 15 ml), and the organic phase was washed with 5% $NaHCO_3$ (2 × 10 ml) and brine (2 × 10 ml), then dried over $MgSO_4$. Evaporation of the solvent under vacuum afforded 3-*tert*-butyl-5-chloromethyl-2-hydroxybenzaldehyde (**B**) as a yellow crystalline solid (3.4 g, 99% yield). ^{1}H NMR ($CDCl_3$, 300 MHz): δ (ppm) 1.43 (s, 9H), 4.59 (s, 2H), 7.44 (d, 1H), 7.53 (d, 1H), 9.87 (s, 1H), 11.87 (s, 1H).

The monotartarate salt of (1*R*, 2*R*)-(-)-1,2-diaminocyclohexane (1.6 g, 6 mmol) and compound **B** (2.7 g, 12 mmol) were refluxed for 3 h with K_2CO_3 (1.7 g, 12.3 mmol) in absolute ethanol (45 ml) under stirring. The reaction mixture was cooled to room temperature, and 12.5 ml of deionized water was added. The mixture was kept at 273–277 K for 12 h, after which the yellow precipitate was collected by filtration. The crude solid was redissolved in dichloromethane (50 ml) and washed with deionized water (2 × 15 ml) and brine (10 ml). After drying over $MgSO_4$, the solvent was removed under vacuum, after which the chiral ligand **C** was isolated as a yellow creamy solid (2.7 g, 85% yield). ^{1}H NMR ($CDCl_3$, 300 MHz): δ (ppm) 1.40 (s, 18H), 1.45–1.99 (m, 8H), 3.30–3.33 (m, 2H), 4.32 (s, 4H), 6.97 (d, 2H), 7.20 (d, 2H), 8.27 (s, 2H), 13.87 (bs, 2H); ^{13}C {^{1}H} NMR (75 MHz in $CDCl_3$): δ (ppm) 24.5, 29.6, 33.3, 35.0, 65.6, 72.6, 72.9, 118.4, 127.6, 129.7, 137.4, 160.2, 165.7.

Ligand **C** (2.7 g, 5 mmol) and $Mn(OAc)_2{\cdot}4H_2O$ (3.7 g, 15 mmol) were dissolved in absolute ethanol (100 ml), and the resulting mixture was refluxed for 0.5 h. Then LiCl (0.6 g, 15 mmol) was added, and the mixture was refluxed for an additional 2.5 h under exposure to air. After the reaction mixture was cooled to room temperature, the solvent was completely removed under vacuum. The residue was dissolved in dichloromethane (100 ml) and washed with deionized water (3 × 25 ml) and brine (2 × 20 ml). After drying over $MgSO_4$, the solution was evaporated under vacuum, and the residue was recrystallized from dichloromethane-hexane to give **1** as a brown solid. Elemental analysis calcd (%) for $C_{30}H_{38}N_2O_2MnCl_3$: C, 58.12; H, 6.18; N, 4.52; found: C, 58.42; H, 6.22; N, 4.50; FAB-MS m/z: calcd ($C_{30}H_{38}N_2O_2MnCl_3$) 618.1, found 618.0; FT-IR (KBr): 3009, 2947, 2865, 1610, 1543, 1438, 1388, 1343, 1312, 1266, 1235, 1204, 1166, 1090, 829, 782, 564 cm^{-1}; DR UV–vis: 286, 325, 438, 510 nm.

2.4. Heterogenization of chiral Mn(III) salen complex *1*

The synthesis process is shown as Scheme 1. A suspension of 3-aminopropyltriethoxysilane (0.6 ml) and calcined siliceous mesoporous support (1.0 g) in 100 ml of toluene was stirred under refluxing for 8 h. The resulting solid was filtered, washed thoroughly with ethanol and diethyl ether, and then dried at 313 K under vacuum for 12 h. The dried 3-aminopropylsilyl-functionalized material (1.0 g) was added to a solution of complex **1** (0.12 g) in 50 ml of toluene. The mixture was refluxed under stirring for 24 h. The brown solid products were collected by filtration, washed with diethyl ether, and Soxhlet-extracted with dichloromethane for 24 h. According to the difference of the supports, the heterogeneous catalysts were marked as *n***M48-1** ($n = 12$, 14, 16) and *n***M41-1** ($n = 12$, 14, 16, 18). The content of aminopropyl groups in their modified supports was ca. 2.0 mmol/g as determined by elemental analysis, and the loading of complex **1** in the heterogeneous catalysts was in the range of 0.11–0.13 mmol/g based on Mn element analysis by ICP-AES.

2.5. Asymmetric epoxidation of unfunctionalized olefins

To quantitatively compare the catalytic performance, the amount of heterogeneous catalysts was normalized based on the same amount of Mn(III) salen complex. Enantioselective epoxidation reactions were carried out using catalysts **1**, *n***M48-1** and *n***M41-1** (0.02 mmol, 2 mol%, based on Mn element) with styrene, α-methylstyrene, indene, and 1-phenylcyclohexene as substrates (1 mmol) and *m*-CPBA (2 mmol) as an oxidant in 10 ml of dichloromethane containing toluene (40 μl) as an internal standard and NMO (5 mmol) as an axial base at 273 K. Once the reaction was complete, the supported catalysts were separated by filtration, and the filtrate was washed with 1 N NaOH (10 ml) and brine (10 ml), then dried over $MgSO_4$. The conversions and ee values were determined by GC, with toluene as an internal standard. The filtrate was detected by ICP-AES,

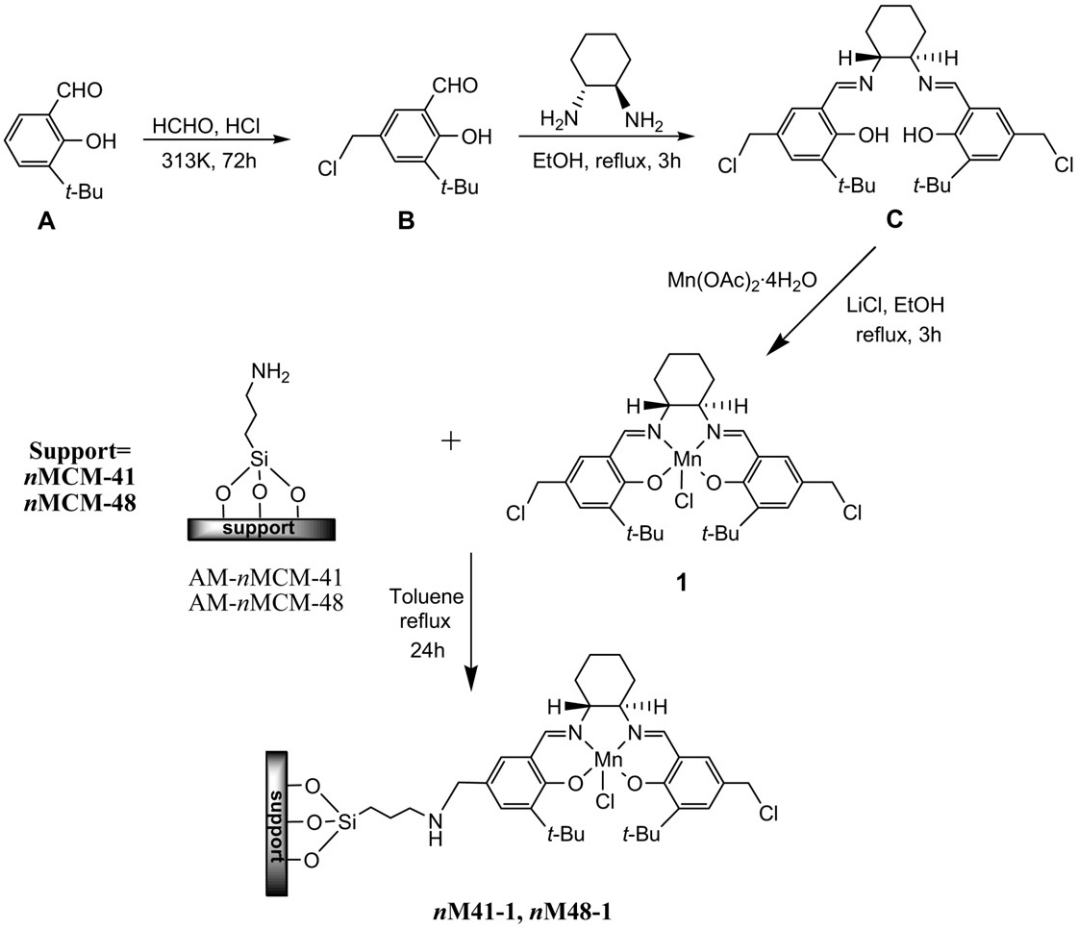

Scheme 1. The synthesis of chiral Mn(III) salen complex **1** and heterogeneous catalysts *n*M**41-1** and *n*M**48-1**.

and only a slight Mn leaching (<1.5%) was found. Moreover, it showed no further increase in the conversion while fresh reactant was being added to the filtrate.

3. Results and discussion

3.1. Characterization of the supports

The synthesized mesoporous materials *n*MCM-41 and *n*MCM-48 were characterized by XRD and N_2 sorption. Fig. 1 shows the powder XRD patterns of calcined *n*MCM-41 and *n*MCM-48. The mesoporous materials *n*MCM-41 exhibited three XRD peaks corresponding to (100), (110), and (200) reflections, which can be indexed to a two-dimensional hexagonal lattice (Fig. 1A). The XRD patterns of *n*MCM-48 (Fig. 1B) showed a very intense peak assigned to reflection at (211) along with a shoulder peak at reflection (220) and the sextet patterns observed in the region of 3°–6° that could be attributed to reflections (321), (400), (420), (332), (422), and (431), which are typical for cubic cells. Moreover, with the decreased alkyl chain length of the templates, the XRD peak at (100) in Fig. 1A and the XRD peak at (211) in Fig. 1B were shifted to higher 2θ values.

Fig. 2 shows the pore size distributions of calcined *n*MCM-41 and *n*MCM-48 materials. It can be seen that all of the synthesized *n*MCM-41 and *n*MCM-48 materials have uniform pore sizes and that their pore sizes regularly decrease with decreasing alkyl chain length of the templates.

3.2. Characterization of the heterogeneous catalysts

3.2.1. Powder X-ray diffraction

The powder XRD patterns of the calcined supports (16MCM-41 and 16MCM-48), the 3-aminopropyltriethoxysilane-modified supports (AM-16MCM-41 and AM-16MCM-48), and the heterogeneous catalysts (**16M41-1** and **16M48-1**) are shown in Fig. 3. Although a slight decrease in the relative intensities of the XRD reflections can be seen, the well-resolved reflections (110) and (200) for AM-16MCM-41 and reflection (220) for AM-16MCM-48 indicate that the mesoporous structure of the parent supports remained intact on modification with 3-aminopropyltriethoxysilane. After the immobilization of chiral Mn(III) salen complex **1**, the intensities of all peaks decreased. However, the XRD pattern of immobilized catalyst showed a similar periodic structure to that of the corresponding support. These findings demonstrate that 3-aminopropyltriethoxysilane modification and chiral Mn(III) salen complex **1** immobilization had little effect on the long-range mesoporous ordering of parent supports.

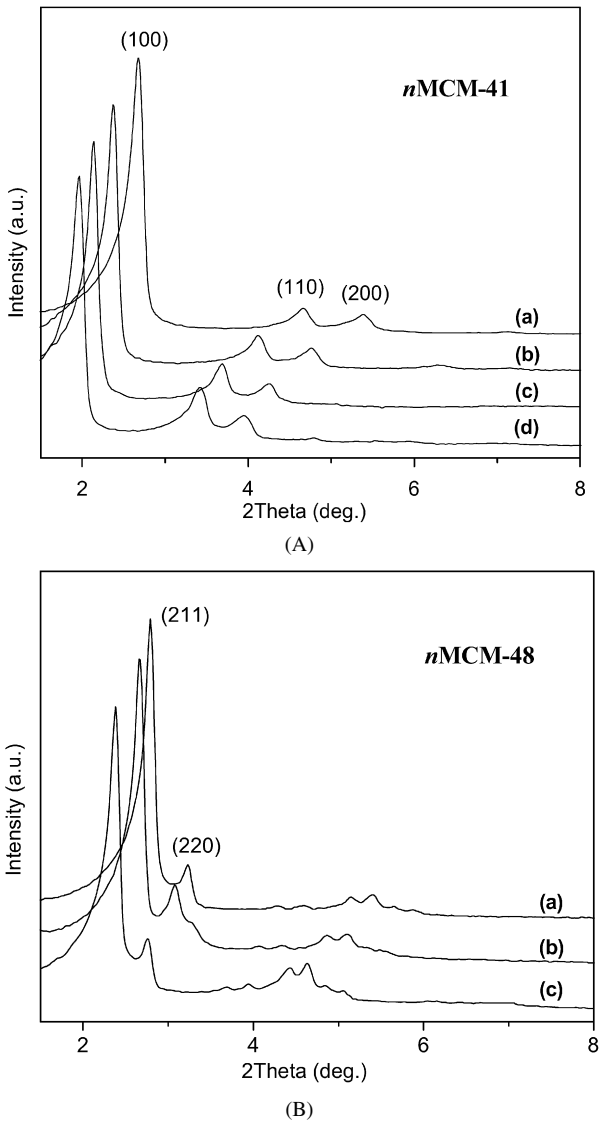

Fig. 1. (A) Powder XRD patterns of calcined *n*MCM-41, (a) $n = 12$, (b) $n = 14$, (c) $n = 16$, (d) $n = 18$. (B) Powder XRD patterns of calcined *n*MCM-48, (a) $n = 12$, (b) $n = 14$, (c) $n = 16$.

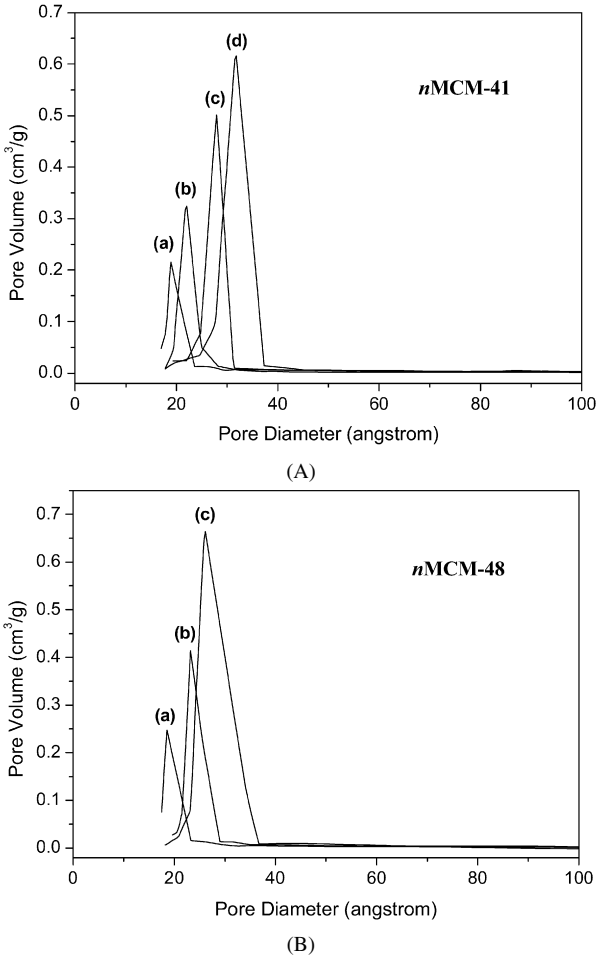

Fig. 2. (A) Pore diameter distributions of calcined *n*MCM-41, (a) $n = 12$, (b) $n = 14$, (c) $n = 16$, (d) $n = 18$. (B) Pore diameter distributions of calcined *n*MCM-48, (a) $n = 12$, (b) $n = 14$, (c) $n = 16$.

3.2.2. FT-IR spectroscopy

Fig. 4 shows the representative FT-IR spectra in the scan range of 1300–3100 cm^{-1} for the calcined support 16MCM-48, the 3-aminopropyltriethoxysilane-modified support AM-16MCM-48, and the heterogeneous catalyst **16M48-1**. The intensities of the bands near 3000 cm^{-1}, which were due to C–H stretching vibrations of alkyl groups, increased with the modification of 3-aminopropyltriethoxysilane and the immobilization of chiral Mn(III) salen complex **1**. In the spectrum of AM-16MCM-48, the IR bands at 1560 and 1470 cm^{-1} could be assigned to N–H deformation vibrations of amido groups and scissor bending vibrations of the $–CH_2–CH_2–CH_2–$groups, respectively. Moreover, the bands at 1420 and 1389 cm^{-1} were attributed to C–H deformation vibrations of alkyl groups. On immobilization of Mn(III) salen complex **1**, two new characteristic IR bands appeared at 1540 and 1450 cm^{-1}, which were due to the stretching vibrations of azomethine groups (H–C=N) and the deformation vibrations of C–H bond, respectively. The FT-IR spectra confirmed the successful modification of the mesoporous support with 3-aminopropyltriethoxysilane and immobilization of chiral Mn(III) salen complex **1**.

3.2.3. UV–vis spectroscopy

The diffuse-reflectance UV–vis spectra of chiral Mn(III) salen complex **1**, the mesoporous supports (18MCM-41 and 14MCM-48), and the heterogeneous catalysts (**18M41-1** and **14M48-1**) are shown in Fig. 5. The spectra of heterogeneous catalysts **18M41-1** and **14M48-1** showed features similar to those of complex **1**, with no obvious absorption in the spectra of 14MCM-48 and 18MCM-41. In the spectrum of chiral Mn(III) salen complex **1**, the bands at 286 and 325 nm could be attributed to the charge transfer transition of salen ligand, the band at 438 nm was due to ligand-to-metal charge transfer transition, and the band at 510 nm may be assigned to the *d–d* transition of Mn(III) salen complex. After immobilization of Mn(III) salen complex on mesoporous materials, all of the characteristic bands appeared in the spectra. But a blue shift from 286 and 438 nm to 260 and 408 nm, respectively, indicated the presence of interaction between Mn(III) salen complex and the support. The DR UV–vis spectra further confirmed the immobilization of chiral Mn(III) salen complex **1** on the supports.

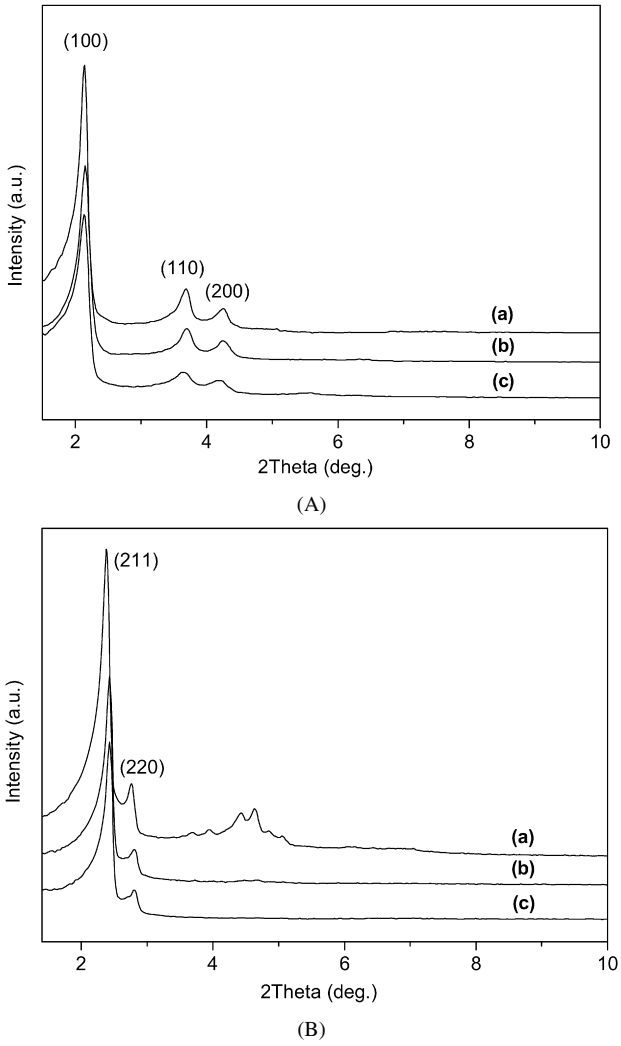

Fig. 3. (A) Powder XRD patterns of (a) calcined 16MCM-41, (b) AM-16MCM-41, (c) **16M41-1**. (B) Powder XRD patterns of (a) calcined 16MCM-48, (b) AM-16MCM-48, (c) **16M48-1**.

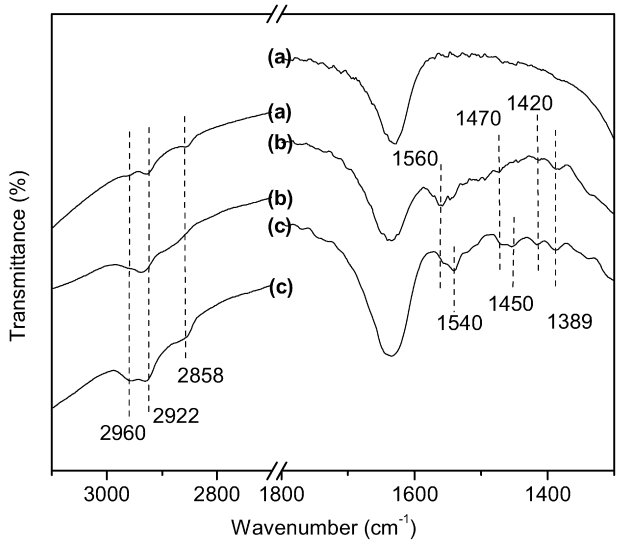

Fig. 4. FT-IR spectra of (a) calcined 16MCM-48, (b) AM-16MCM-48, (c) **16M48-1**.

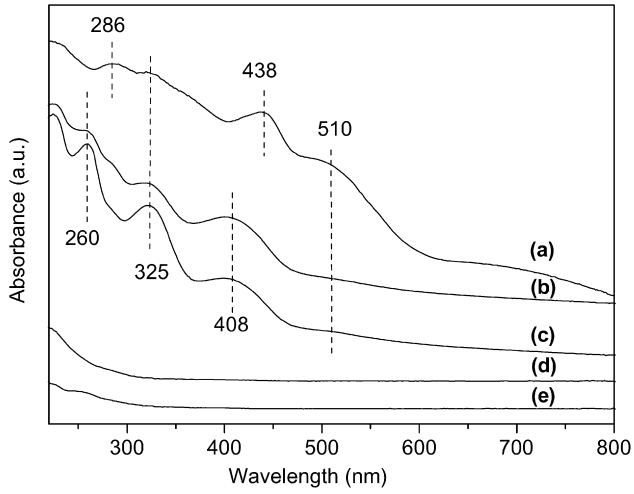

Fig. 5. Diffuse-reflectance UV–vis spectra of (a) Mn(III) salen complex **1**, (b) **14M48-1**, (c) **18M41-1**, (d) calcined 14MCM-48, (e) calcined 18MCM-41.

Table 1
The structure parameters of parent supports and heterogeneous catalysts

Sample	S_{BET} ($m^2\,g^{-1}$)	Pore volume ($cm^3\,g^{-1}$)	Pore size (Å)
18MCM-41	1112	1.11	31.7
18M41-1	577	0.45	21.2
16MCM-41	941	0.82	27.9
16M41-1	556	0.39	18.8
14MCM-41	841	0.71	21.9
14M41-1	477	0.29	18.6
12MCM-41	873	0.59	18.9
12M41-1	691	0.32	17.1
16MCM-48	1200	1.11	26.0
16M48-1	991	0.56	19.9
14MCM-48	1201	0.80	23.2
14M48-1	667	0.29	19.0
12MCM-48	1257	0.82	18.6
12M48-1	546	0.25	17.0

3.2.4. Nitrogen sorption

All of the parent supports and the heterogeneous catalysts were characterized by N_2 sorption. The corresponding textural parameters calculated by N_2 adsorption–desorption isotherms are presented in Table 1. Compared with parent supports, a large decrease in BET surface area, pore volume, and pore size was observed on immobilization of chiral Mn(III) salen complex **1** onto mesoporous materials. This evidences that the chiral Mn(III) salen complexes are located mainly on the inner surfaces of the supports. Fig. 6 shows the low-temperature N_2 adsorption–desorption isotherms and the pore size distributions of the heterogeneous catalysts **18M41-1** and **16M48-1**. It can be seen that the immobilized catalysts maintained characteristic type IV isotherms [33] and uniform pore size in the mesopore ranges.

3.3. Heterogeneous asymmetric epoxidation

The heterogeneous catalysts were evaluated in the epoxidation of styrene, α-methylstyrene, indene, and 1-phenylcyclohexene in CH_2Cl_2 at 273 K for 8 h using *m*-CPBA/NMO as

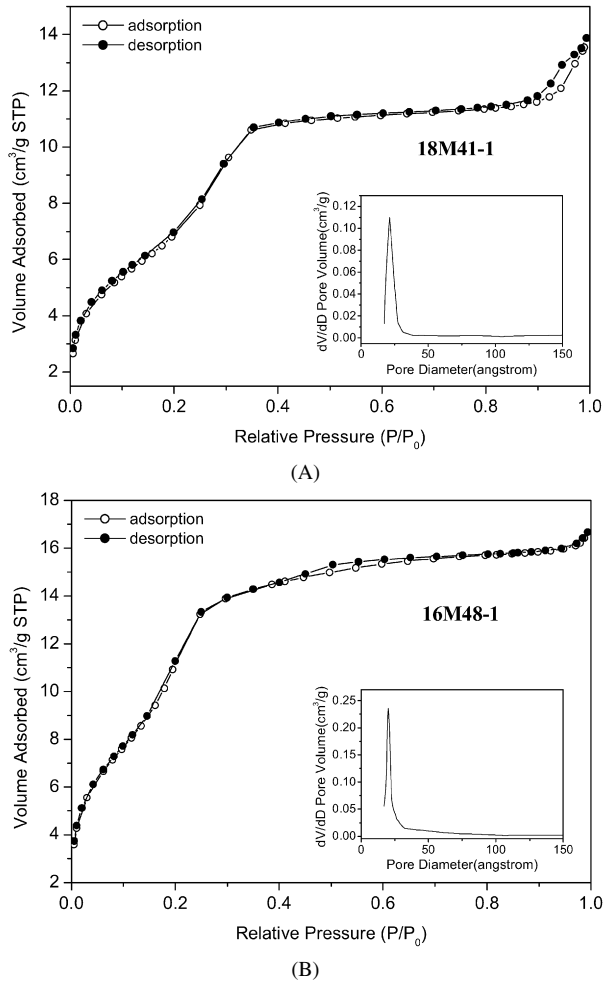

Fig. 6. N_2 adsorption–desorption isotherms and pore diameter distribution profiles (insert) of (A) **18M41-1**, (B) **16M48-1**.

the oxidant. The blank experiments showed that the asymmetric epoxidation hardly occurred in the absence of chiral Mn(III) salen complex. For comparison, the chiral Mn(III) salen catalyst **1** was also investigated under the same reaction conditions, but shortening the reaction time to 2 h.

Table 2 gives the results of the asymmetric epoxidation of styrene and α-methylstyrene catalyzed by homogeneous and heterogeneous catalysts. The catalysts **18M41-1**, **16M41-1**, **16M48-1**, and **14M48-1** were active and enantioselective for the epoxidation of styrene and α-methylstyrene, and conversions and ee values comparable to those of homogeneous catalyst **1** were obtained (entries 2, 3, 6, 7, 10, 11, 14, and 15), which was attributed mainly to the large pore sizes of the corresponding supports. The size of the Mn(III) salen complex **1** was estimated as 2.0 × 1.6 nm according to the literature [14,34]. The mesoporous materials 18MCM-41, 16MCM-41, 16MCM-48, and 14MCM-48 had pore sizes >2.3 nm, sufficiently large for the immobilization of the chiral Mn(III) salen complex **1** into the channels of supports. The catalyst **18M41-1** showed higher conversions and ee values for the epoxidation of styrene and α-methylstyrene compared with those of **16M41-1** (entries 2, 3, 10, and 11). However, compared with **16M48-1**, catalyst **14M48-1** exhibited lower conversions and higher ee values for

Table 2
Asymmetric epoxidation of styrene and α-methylstyrene catalyzed by homogeneous complex **1** and heterogeneous catalysts[a]

Entry	Catalyst	Substrate	Time (h)	Conversion (%)[b]	Ee (%)[c]
1	**1**	Styrene	2	>99	49.0 (*R*)
2	**18M41-1**		8	>99	49.0 (*R*)
3	**16M41-1**		8	97.2	48.0 (*R*)
4	**14M41-1**		8	79.6	36.0 (*R*)
5	**12M41-1**		8	72.2	28.8 (*R*)
6	**16M48-1**		8	>99	47.7 (*R*)
7	**14M48-1**		8	>99	49.0 (*R*)
8	**12M48-1**		8	47.6	15.3 (*R*)
9	**1**	α-Methylstyrene	2	>99	41.8 (*R*)
10	**18M41-1**		8	>99	39.5 (*R*)
11	**16M41-1**		8	95.7	38.5 (*R*)
12	**14M41-1**		8	80.1	32.9 (*R*)
13	**12M41-1**		8	67.7	29.4 (*R*)
14	**16M48-1**		8	>99	37.2 (*R*)
15	**14M48-1**		8	>99	40.4 (*R*)
16	**12M48-1**		8	29.0	25.1 (*R*)

[a] Reactions were performed in CH_2Cl_2 (10 ml) with catalyst (0.02 mmol), substrate (1 mmol), NMO (5 mmol), and *m*-CPBA (2 mmol) at 273 K.
[b] Conversion (%) determined by GC with chiral column using toluene as internal standard.
[c] Ee (%) determined by GC with RESTEK RT-BetaDEXse chiral column.

styrene and α-methylstyrene epoxidation (entries 6, 7, 14, and 15). This may be due to the confinement effect of the nanopores of 14MCM-48, which was more compatible with the molecular size of styrene and α-methylstyrene.

As shown in Table 2, the heterogeneous catalysts **14M41-1**, **12M41-1**, and **12M48-1** demonstrated lower activity and enantioselectivity (entries 4, 5, 8, 12, 13, and 16) compared with the homogeneous catalyst **1** and the other four kinds of heterogeneous catalysts, due mainly to the small pore sizes of the corresponding supports. The results of N_2 sorption (Table 1) indicate that the BET surface area, pore volume, and pore diameter were obviously decreased on immobilization of chiral Mn(III) salen complex **1** onto the parent supports 14MCM-41, 12MCM-41, and 12MCM-48, indicating that the chiral Mn(III) salen complex **1** was present inside the channels of these supports. However, the blockage of pore channels by the Mn(III) salen complex could occur. Moreover, the relatively small pore size of the obtained catalysts would increase the diffusional resistance of reactants to the active sites located on the inner surfaces of the supports. Thus, these catalysts exhibited decreased performance. In particular, the lowest catalytic activities and enantionselectivities (e.g., 47.6% conversion and 15.3% ee value for styrene epoxidation) were provided by the catalyst immobilized on 12MCM-48, which had the smallest pore diameter among the parent supports.

In summary, the catalytic performance of heterogeneous catalysts was closely correlated with the pore sizes of the parent supports for the epoxidation of styrene and α-methylstyrene. For the catalysts *n***M41-1**, the activity and enantioselectivity were improved with the increasing pore sizes of the parent supports. The catalyst **18M41-1** exhibited the best catalytic performance (e.g., >99% conversion and 49.0% ee value for styrene epoxidation). For the catalysts *n***M48-1**, with an increase in pore

Table 3
Asymmetric epoxidation of indene and 1-phenylcyclohexene catalyzed by homogeneous complex **1** and heterogeneous catalysts[a]

Entry	Catalyst	Substrate	Time (h)	Conversion (%)[b]	Ee (%)[c]
1	**1**	Indene	2	99.0	91.0 (1*R*, 2*S*)
2	**18M41-1**		8	96.9	87.8 (1*R*, 2*S*)
3	**16M41-1**		8	96.7	87.0 (1*R*, 2*S*)
4	**14M41-1**		8	78.8	73.3 (1*R*, 2*S*)
5	**12M41-1**		8	77.3	62.5 (1*R*, 2*S*)
6	**16M48-1**		8	97.5	89.1 (1*R*, 2*S*)
7	**14M48-1**		8	97.3	93.3 (1*R*, 2*S*)
8	**12M48-1**		8	52.4	50.4 (1*R*, 2*S*)
9	**1**	1-Phenylcyclohexene	2	>99	83.9 (1*S*, 2*S*)
10	**18M41-1**		8	93.2	78.7 (1*S*, 2*S*)
11	**16M41-1**		8	79.8	60.7 (1*S*, 2*S*)
12	**14M41-1**		8	37.6	38.3 (1*S*, 2*S*)
13	**12M41-1**		8	23.2	34.6 (1*S*, 2*S*)
14	**16M48-1**		8	98.9	79.6 (1*S*, 2*S*)
15	**14M48-1**		8	73.8	70.6 (1*S*, 2*S*)
16	**12M48-1**		8	23.0	16.0 (1*S*, 2*S*)

[a] Reactions were performed in CH_2Cl_2 (10 ml) with catalyst (0.02 mmol), substrate (1 mmol), NMO (5 mmol), and *m*-CPBA (2 mmol) at 273 K.
[b] Conversion (%) determined by GC with chiral column using toluene as internal standard.
[c] Ee (%) determined by GC with RESTEK RT-BetaDEXse chiral column.

size, the conversions increased from 47.6 to >99% for styrene epoxidation and from 29.0 to >99% for α-methylstyrene epoxidation. However, the compatible pore size may be responsible for the improved ee values, and the catalyst **14M48-1** exhibited the highest ee value for the epoxidation of styrene and α-methylstyrene.

Table 3 gives the results of the asymmetric epoxidation of indene and 1-phenylcyclohexene catalyzed by homogeneous and heterogeneous chiral Mn(III) salen catalysts. Similarly, the immobilized catalysts based on the large–pore size mesoporous supports showed conversions and ee values comparable with those of the homogeneous catalyst **1** (entries 2, 3, 6, 7, 10, 11, 14, and 15), and the catalysts supported by the small pore size mesoporous materials showed relatively lower activity and enantioselectivity (entries 4, 5, 8, 12, 13, and 16). For the catalysts *n***M41-1**, the activity and enantioselectivity decreased with reduced pore sizes of the parent supports for the epoxidation of indene and 1-phenylcyclohexene. Moreover, for the catalysts *n***M48-1**, the large pore size could lead to higher conversions, and the compatible pore size was beneficial to obtain the increased ee values. As shown in Table 3, the heterogeneous catalyst **14M48-1** exhibited the highest ee value of 93.3% (entry 7) for the epoxidation of indene, which was higher than that of the homogeneous counterpart (91.0% ee, entry 1). The catalyst **16M48-1** obtained the best enantioselectivity for the epoxidation of 1-phenylcyclohexene (79.6% ee, entry 14). This may be explained by the fact that 1-phenylcyclohexene has a larger molecular size than the other substrates, and thus the catalyst **16M48-1** with large pore size was more compatible with the size of 1-phenylcyclohexene and exhibited the best enantioselectivity. These results further confirm the presence of the confinement effect of nanopores.

4. Conclusion

The chiral Mn(III) salen complex was immobilized onto a series of mesoporous materials with different pore sizes. The as-synthesized catalysts were active and enantioselective for the epoxidation of styrene, α-methylstyrene, indene, and 1-phenylcyclohexene. The effects of pore size on the activity and enantioselectivity of the heterogeneous catalysts were studied. For the catalysts immobilized on *n*MCM-41 materials, the catalytic activity and enantioselectivity were improved with the increase of pore sizes of parent supports. The heterogeneous catalyst **18M41-1** gave the highest conversions and ee values for the epoxidation of olefins. And for the *n*MCM-48 material-supported catalysts, the large pore size was beneficial to obtain higher catalytic activity, and the compatible pore size may have been responsible for the increased enantioselectivity in the olefin epoxidation. The catalyst **14M48-1** exhibited the best enantioselectivity for the epoxidation of styrene, α-methylstyrene, and indene. In particular, a higher ee value than the homogeneous ee (93.3 vs 91.0%) was achieved for indene epoxidation. However, the highest ee value for the epoxidation of 1-phenylcyclohexene was provided by the catalyst **16M48-1**.

Acknowledgments

This work was supported by the National Natural Science Foundation of China (grants 20773069 and 29973016) and the National Key Technologies R&D Program of China (grant 2006BAC02A12).

References

[1] H. Zhang, C. Li, Tetrahedron 62 (2006) 6640.
[2] W. Zhang, J.L. Loebach, S.R. Wilson, E.N. Jacobsen, J. Am. Chem. Soc. 112 (1990) 2801.
[3] K. Srinivasan, P. Michaud, J.K. Kochi, J. Am. Chem. Soc. 108 (1986) 2309.
[4] C. Baleizão, H. Garcia, Chem. Rev. 106 (2006) 3987.
[5] L. Canali, D.C. Sherrington, Chem. Soc. Rev. 28 (1999) 85.
[6] N.E. Leadbeater, M. Marco, Chem. Rev. 102 (2002) 3217.
[7] Q.-H. Fan, Y.-M. Li, A.S.C. Chan, Chem. Rev. 102 (2002) 3385.
[8] C. Bianchini, P. Barbaro, Top. Catal. 19 (2002) 17.
[9] C.-E. Song, S.-G. Lee, Chem. Rev. 102 (2002) 3495.
[10] P. McMorn, G.J. Hutchings, Chem. Soc. Rev. 33 (2004) 108.
[11] C. Li, Catal. Rev.-Sci. Eng. 46 (2004) 419.
[12] C. Li, H. Zhang, D. Jiang, Q. Yang, Chem. Commun. (2007) 547.
[13] H. Zhang, S. Xiang, C. Li, Chem. Commun. (2005) 1209.
[14] H. Zhang, Y. Zhang, C. Li, J. Catal. 238 (2006) 369.
[15] R.I. Kureshy, I. Ahmad, N.H. Khan, S.H.R. Abdi, S. Singh, P.H. Pandia, R.V. Jasra, J. Catal. 235 (2005) 28.
[16] R.I. Kureshy, I. Ahmad, N.H. Khan, S.H.R. Abdi, K. Pathak, R.V. Jasra, J. Catal. 238 (2006) 134.
[17] L.-L. Lou, K. Yu, F. Ding, W. Zhou, X. Peng, S. Liu, Tetrahedron Lett. 47 (2006) 6513.
[18] L.-L. Lou, K. Yu, F. Ding, X. Peng, M. Dong, C. Zhang, S. Liu, J. Catal. 249 (2007) 102.
[19] G.-J. Kim, J.-H. Shin, Tetrahedron Lett. 40 (1999) 6827.
[20] K. Yu, L.-L. Lou, F. Ding, S. Wang, Z. Wang, S. Liu, Catal. Commun. 7 (2006) 170.
[21] K. Yu, L.-L. Lou, C. Lai, S. Wang, F. Ding, S. Liu, Catal. Commun. 7 (2006) 1057.
[22] G.-J. Kim, S.-H. Kim, Catal. Lett. 57 (1999) 139.

[23] P. Piaggio, C. Langham, P. McMorn, D. Bethell, P.C.B. Page, F.E. Hancock, C. Sly, G.J. Hutchings, J. Chem. Soc. Perkin Trans. 2 (2000) 143.
[24] P. Piaggio, P. McMorn, D. Murphy, D. Bethell, P.C.B. Page, F.E. Hancock, C. Sly, O.J. Kerton, G.J. Hutchings, J. Chem. Soc. Perkin Trans. 2 (2000) 2008.
[25] J.M. Thomas, T. Maschmeyer, B.F.G. Johnson, D.S. Shephard, J. Mol. Catal. A Chem. 141 (1999) 139.
[26] N.A. Caplan, F.E. Hancock, P.C.B. Page, G.J. Hutchings, Angew. Chem. Int. Ed. 43 (2004) 1685.
[27] G. Casiraghi, G. Casnati, M. Cornia, A. Pochini, G. Puglia, G. Sartori, R. Ungaro, J. Chem. Soc. Perkin Trans. 1 (1978) 318.
[28] J.F. Larrow, E.N. Jacobsen, Y. Gao, Y. Hong, X. Nie, C.M. Zepp, J. Org. Chem. 59 (1994) 1939.
[29] H. Zhang, S. Xiang, J. Xiao, C. Li, J. Mol. Catal. A Chem. 238 (2005) 175.
[30] C.T. Kresge, M.E. Leonowicz, W.J. Roth, J.C. Vartuli, J.S. Beck, Nature 359 (1992) 710.
[31] J.S. Beck, J.C. Vartuli, W.J. Roth, M.E. Leonowicz, C.T. Kresge, K.D. Schmitt, C.T.-W. Chu, D.H. Olson, E.W. Sheppard, S.B. McCullen, J.B. Higgins, J.L. Schlenker, J. Am. Chem. Soc. 114 (1992) 10834.
[32] L. Canali, E. Cowan, H. Deleuze, C.L. Gibson, D.C. Sherrington, J. Chem. Soc. Perkin Trans. 1 (2000) 2055.
[33] K.S.W. Sing, D.H. Everett, R.A.W. Haul, L. Moscou, R.A. Pierotti, J. Rouquerol, T. Siemieniewska, Pure Appl. Chem. 57 (1985) 603.
[34] A.R. Silva, V. Budarin, J.H. Clark, B. Castro, C. Freire, Carbon 43 (2005) 2096.